

The size and geometry of the Ly α clouds [★]

V. D’Odorico¹, S. Cristiani², S. D’Odorico³, A. Fontana⁴, E. Giallongo⁴, and P. Shaver³

¹ International School for Advanced Studies, SISSA, via Beirut 2-4, I-34014 Trieste, Italy

² Dipartimento di Astronomia dell’Università di Padova, Vicolo dell’Osservatorio 5, I-35122 Padova, Italy

³ European Southern Observatory, Karl Schwarzschild Strasse 2, D-85748 Garching, Germany

⁴ Osservatorio Astronomico di Roma, via dell’Osservatorio, I-00040 Monteporzio, Italy

Received April 16, 1998; accepted . . .

Abstract. Spectra of the QSO pair Q0307-195A,B have been obtained in the Ly α forest (3660–3930 Å) and C IV (4720–4850 Å) regions with a FWHM resolution between 0.7 and 0.5 Å. 46 lines have been detected in the spectrum of object A while 36 in the spectrum of object B, of them 29 and 20 were identified as Ly α absorptions respectively. The present observations have been supplemented with data of comparable quality on other 7 QSO pairs available in the literature to give an enlarged sample of 217 Ly α lines with rest equivalent width $W_o \geq 0.3$ Å. The analysis of the hits (i.e. when an absorption line appears in both QSO spectra) and misses (i.e. when a line is seen in any of the QSO spectra, but no line is seen in the other), carried out with an improved statistical approach, indicates that the absorbers have typically a large size¹: $R = 362 h^{-1}$ kpc, with 95% confidence limits $298 < R < 426 h^{-1}$ kpc and $R = 412 h^{-1}$ kpc, with 95% confidence limits $333 < R < 514 h^{-1}$ kpc for the radius of idealized spherical and disc geometries, respectively. The present data do not allow to establish any correlation of the typical inferred size with the proper separation or with the redshift of the pairs.

The correlation between the observed equivalent widths of the absorbers in the adjacent lines of sight becomes poorer and poorer with increasing proper separation. A disc geometry with a column density profile $N(r) \propto (r/R_0)^{-\gamma}$, $\gamma = 4$, is found to reasonably reproduce the data with $R_0 \simeq 100 - 200 h^{-1}$ kpc, but also spherical clouds with the same column density profile and a power-law distribution of radii may give a satisfactory representation of the observations.

Key words: intergalactic medium – quasars: absorption lines – quasars:individual(Q0307-195A,B)

Send offprint requests to: Stefano Cristiani

[★] Based on observations collected at the European Southern Observatory, La Silla, Chile (ESO No. 149.B-0013).

¹ Throughout this paper we will assume: $h \equiv H_0/(100 \text{ km s}^{-1} \text{ Mpc}^{-1})$, $q_0 = 0.5$.

1. Introduction

Closely separated QSO pairs and gravitationally lensed QSOs provide two or more adjacent lines of sight (LOS), which allow to sample the size and clustering of the absorbers.

The ray path separation of gravitationally lensed QSOs usually spans subgalactic scales; studies of these spectra have shown that the Ly α clouds are much larger than a few kiloparsecs (Weymann & Foltz 1983; Foltz et al. 1984; Smette et al. 1992, 1995). Further results again pointing at very large sizes have been obtained for LOS separations of a few arcminutes or less (Shaver & Robertson 1983, SR83; Crofts 1989; Dinshaw et al. 1995; Dinshaw et al. 1997, D97; Fang et al. 1996, FDCB; Crofts & Fang 1997, CF97). The first indication in this sense has been obtained observing the QSO pair Q1343+2640A,B (with a proper sightline separation of $39-40 h^{-1}$ kpc at $z \sim 2$), indicating a cloud radius of $100 - 200 h^{-1}$ kpc (Bechtold et al. 1994; Dinshaw et al. 1994). QSO pairs with separations larger than a few arcminutes, corresponding to proper separations up to megaparsecs, have the potential to study the large-scale spatial distribution of Ly α or metal absorbers (Crofts 1985; Jakobsen et al. 1986; Tytler, Sandoval & Fan 1993; Elowitz, Green & Impey 1995; Dinshaw & Impey 1996; Williger et al. 1996).

Multiple sightlines are also highly valuable in probing the large scale structure. In particular, multiple, well-sampled sightlines can provide a stronger test for voids by placing more absorbers in a void-sized volume than could possibly be obtained along a single sightline.

Furthermore, the effect of the UV radiation field of a foreground QSO on the absorption spectrum of a background QSO provides an important way of testing the “proximity effect” interpretation (Bajtlik, Duncan & Ostriker 1988) of the “inverse effect” observed in single QSO sightlines.

We present new observations of the QSO pair Q0307-195A,B discovered in an objective prism survey by MacAlpine and Feldman (1982) (A = UM 680 and B =

UM 681). Later on, the pair was observed by Shaver and Robertson (1983) who analyzed the absorption spectra of the two objects. Both QSOs are about of 19th magnitude, their redshifts are $z_{\text{em}}(\text{A}) = 2.1439 \pm 0.0003$ and $z_{\text{em}}(\text{B}) = 2.1217 \pm 0.0003$ (SR83), and they are separated by 56 arcseconds on the plane of the sky. The redshift difference is small enough ($\sim 2126 \text{ km s}^{-1}$) that they could be members of the same cluster.

The rest of the paper is organized as follows: in § 2, we present spectroscopic observations of Q0307-195A,B and describe the procedure of reduction and calibration of the spectra. In § 3 the metallic systems in the two QSO spectra are listed and briefly discussed. Section 4 describes the procedure to obtain an estimate for the radius of the Ly α absorbers in the hypothesis of simple geometry. In subsection 4.1 we tackle the same issue on the basis of more realistic models for the absorbers. Finally, in § 5 we summarize our results.

2. Observations and data reduction

We obtained spectra of the QSO pair Q0307-195A,B with the blue arm of the EMMI spectrograph at the 3.5m New Technology Telescope of the European Southern Observatory in two runs in November 1994 and November 1995. The spectrograph was used with the holographic 3000 lines mm^{-1} grating (ESO # 11) and a 1024^2 , $24 \mu\text{m}$ pixel, Tektronix CCD (ESO # 31). Two or three spectra were obtained at each of three different central wavelengths: 3690,3750 and 3850 Å (Ly α forest region) and one at 4780 Å (C IV region). Typical exposure times were 6000 s/spectrum for a total exposure time of 56 900 s. In this instrument configuration one CCD pixel corresponds on average to 0.15 and 0.13 Å in the UV and blue regions respectively. The typical slit width was 1.2 arcsec in width and 180 arcsec in length and it was aligned at P.A. $135^\circ.6$ to capture both QSOs.

The spectra were extracted, wavelength calibrated, normalized and merged using standard procedures of the ESO MIDAS *long slit* reduction package.

The final smoothed and merged spectra cover the ranges $\lambda\lambda 3660 - 3930 \text{ Å}$ and $\lambda\lambda 4720 - 4850 \text{ Å}$.

The resolution, as measured from the Thorium lines of the calibration spectra, extracted and treated in the same way as the QSOs spectra, is 0.7 and 0.5 Å in the UV and blue range respectively. The s/n ratio of the final spectra varies from 25 at the peak of the Ly α emissions of the two QSOs to 5 at the shortest wavelengths. The relative accuracy of the wavelength scales in the spectra of the two QSOs is better than 20 km s^{-1} .

The normalized spectra are shown in Figs. 1, 2.

3. Detection and identification of lines

The determination of the continuum in the QSO spectrum is a critical step because it affects the measurement

of the absorption line parameters. In the present work, we selected the portions of the spectrum free of strong absorption lines or artificial peaks (e.g. due to cosmic rays), i.e. where the RMS fluctuation about the mean becomes consistent with noise statistics, and then, we estimated the continuum level by spline-fitting these regions with quadratic polynomials.

In order to detect the absorption lines we have searched for all the features deviating from the continuum more than 3.5 times the RMS noise. The lines have been fitted with Voigt profiles convolved with the instrumental spread function, making use of a minimization method of χ^2 . This step has been performed within the ESO MIDAS *lyman* package (Fontana & Ballester 1995). The values of the wavelength, redshift z , and rest equivalent width W_o have been determined for isolated lines and individual components of blends.

The number of components of each absorption feature is assumed to be the minimum required to give a reduced $\chi^2 < 1$ (corresponding to a confidence level $P \gtrsim 50\%$).

The error on the observed equivalent widths was computed in such a way that it includes also the uncertainty in the determination of the level of the continuum and in the choice of the fitting interval for the lines.

Due to the improved signal to noise ratio (s/n) and resolution, we observe more than twice the number of lines found by SR83 in the common wavelength interval. The lists of lines are presented in the Tables 1, 2.

3.1. Metal Systems

We based the identification of metal lines on SR83. All the systems reported by them in the common wavelength interval are confirmed, in addition we found one new system in Q0307-195A and one possible new system in Q0307-195B (see 3.2 and 3.3).

An identification programme, based on the method of Young et al. (1979), has been applied to the newly observed lines that could not be attributed to systems already identified by SR83. Because of the limited wavelength coverage in the red region of the spectra, we were able to identify only one new C IV doublet.

Four and five lines redward of the Ly α remained unidentified in Q0307-195A and B respectively.

The metal systems of each object are described in detail in the following section.

3.2. Object Q0307-195A

The metal system at $z_{\text{abs}} = 2.1229 - a$

Already observed by SR83. This absorption system presents a redshift difference of only 115 km s^{-1} with object B and of 77 km s^{-1} with system *a* of object B. SR83 argued that this common absorption is likely due to a very extended gaseous halo or disc, physically associated with Q0307-195B itself.

Table 1. Absorption lines in the spectrum of Q0307-195A

No.	λ (Obs.) (\AA)	W_λ (rest) (\AA)	W_λ (obs) (\AA)	Identification	z_{abs}	Metal System
1	3661.43 \pm 0.04	0.62	1.88 \pm 0.04	Si III (1206)	2.0348	c
2	3663.31 \pm 0.05	0.16	0.48 \pm 0.05	H I (1216)	2.0134	
3	3665.80 \pm 0.05	0.17	0.50 \pm 0.04	H I (1216)	2.0155	
4	3669.36 \pm 0.05	0.33	1.00 \pm 0.10	H I (1216)	2.0184	
5	3676.08 \pm 0.06	0.32	0.97 \pm 0.06	H I (1216)	2.0239	
6	3689.15 \pm 0.02	1.34	4.07 \pm 0.03	H I (1216)	2.0347	c
7	3692.82 \pm 0.03	0.19	0.60 \pm 0.01	H I (1216)	2.0377	
8	3694.16 \pm 0.12	0.23	0.70 \pm 0.06	H I (1216)	2.0388	
9	3699.64 \pm 0.02	0.26	0.81 \pm 0.02	H I (1216)	2.0433	
10	3701.44 \pm 0.04	0.19	0.59 \pm 0.03	H I (1216)	2.0448	
11	3704.01 \pm 0.15	0.20	0.61 \pm 0.02	H I (1216)	2.047	
12	3704.98 \pm 0.08	0.22	0.68 \pm 0.02	H I (1216)	2.0477	
13	3716.92 \pm 0.08	0.34	1.03 \pm 0.04	H I (1216)	2.0575	
14	3719.67 \pm 0.03	0.23	0.71 \pm 0.03	H I (1216)	2.0598	
15	3726.69 \pm 0.04	0.08	0.26 \pm 0.01	H I (1216)	2.0655	
16	3730.29 \pm 0.02	0.41	1.25 \pm 0.01	H I (1216)	2.0685	
17	3751.39 \pm 0.02	0.54	1.68 \pm 0.04	H I (1216)	2.0859	
18	3755.94 \pm 0.18	0.08	0.23 \pm 0.02	H I (1216)	2.089	
19	3757.60 \pm 0.02	0.42	1.29 \pm 0.02	H I (1216)	2.0909	
20	3759.82 \pm 0.03	0.13	0.40 \pm 0.03	H I (1216)	2.0928	
21	3766.09 \pm 0.13	0.49	1.52 \pm 0.02	H I (1216)	2.097	
22	3767.22 \pm 0.02	0.43	1.33 \pm 0.02	H I (1216)	2.0989	b
23	3767.84 \pm 0.06	0.17	0.54 \pm 0.02	Si III (1206)	2.1229	a
24	3770.53 \pm 0.02	0.15	0.45 \pm 0.02	H I (1216)	2.1016	
25	3774.58 \pm 0.04	0.05	0.16 \pm 0.01	H I (1216)	2.1049	
26	3776.67 \pm 0.02	0.16	0.50 \pm 0.03	H I (1216)	2.1066	
27	3779.91 \pm 0.02	0.13	0.41 \pm 0.03	H I (1216)	2.1093	
28	3796.55 \pm 0.01	0.67	2.10 \pm 0.05	H I (1216)	2.1230	a
29	3800.98 \pm 0.01	0.43	1.33 \pm 0.03	H I (1216)	2.1266	
30	3805.15 \pm 0.07	0.03	0.11 \pm 0.01	H I (1216)	2.1301	
31	3817.25 \pm 0.01	0.12	0.37 \pm 0.02	H I (1216)	2.1400	
32	3825.47 \pm 0.01	0.17	0.50 \pm 0.02	Si II (1260)	2.0351	c
33	3838.96 \pm 0.02	0.06	0.19 \pm 0.02	N V (1238)	2.09888	b
34	3851.31 \pm 0.02	0.04	0.13 \pm 0.02	N V (1242)	2.09888	b
35	3867.99 \pm 0.07	-	0.14 \pm 0.02	not ident.		
36	3868.81 \pm 0.01	0.14	0.43 \pm 0.01	N V (1238)	2.12298	a
37	3881.25 \pm 0.01	0.13	0.39 \pm 0.02	N V (1242)	2.12298	a
38	3897.72 \pm 0.06	-	0.51 \pm 0.02	not ident.		
39	3911.83 \pm 0.04	0.36	0.92 \pm 0.05	C IV (1548)	1.5267	d
40	3916.17 \pm 0.04	-	0.23 \pm 0.02	not ident.		
41	3918.34 \pm 0.04	0.30	0.77 \pm 0.05	C IV (1550)	1.5267	d
42	3927.40 \pm 0.02	-	0.58 \pm 0.04	not ident.		
43	4797.22 \pm 0.02	0.24	0.74 \pm 0.03	C IV (1548)	2.0986	b
44	4805.20 \pm 0.02	0.19	0.59 \pm 0.02	C IV (1550)	2.0986	b
45	4834.71 \pm 0.02	0.33	1.03 \pm 0.08	C IV (1548)	2.1228	a
46	4842.75 \pm 0.02	0.23	0.72 \pm 0.04	C IV (1550)	2.1228	a

Table 2. Absorption lines in the spectrum of Q0307-195B

No.	λ (Obs.) (\AA)	W_λ (rest) (\AA)	W_λ (obs) (\AA)	Identification	z_{abs}	System
1	3660.76 \pm 0.47	0.72	2.18 \pm 0.18	Si III (1206)	2.034	b
2	3662.71 \pm 0.15	0.40	1.20 \pm 0.17	H I (1216)	2.0129	
3	3669.45 \pm 0.10	0.54	1.64 \pm 0.04	H I (1216)	2.0185	
4	3672.85 \pm 0.11	0.32	0.96 \pm 0.07	H I (1216)	2.0213	
5	3677.81 \pm 0.08	0.27	0.83 \pm 0.03	H I (1216)	2.0253	
6	3684.11 \pm 0.08	1.16	3.52 \pm 0.04	H I (1216)	2.0305	
7	3687.80 \pm 0.11	1.19	3.62 \pm 0.04	H I (1216)	2.0335	b
8	3693.10 \pm 0.15	0.54	1.65 \pm 0.13	H I (1216)	2.0379	
9	3696.62 \pm 0.05	0.14	0.44 \pm 0.02	H I (1216)	2.0408	
10	3700.04 \pm 0.04	1.25	3.80 \pm 0.04	H I (1216)	2.0436	
11	3703.81 \pm 0.06	0.28	0.85 \pm 0.03	H I (1216)	2.0467	
12	3721.32 \pm 0.04	0.99	3.02 \pm 0.09	H I (1216)	2.0611	
13	3723.77 \pm 0.04	0.49	1.51 \pm 0.09	H I (1216)	2.0631	
14	3730.48 \pm 0.05	0.17	0.53 \pm 0.03	H I (1216)	2.0687	
15	3735.50 \pm 0.05	0.23	0.72 \pm 0.07	H I (1216)	2.0728	
16	3767.14 \pm 0.01	0.64	2.00 \pm 0.04	Si III (1206)	2.1224	a
17	3769.23 \pm 0.10	0.08	0.25 \pm 0.04	H I (1216)	2.1005	
18	3770.50 \pm 0.15	0.10	0.32 \pm 0.04	H I (1216)	2.1016	
19	3775.53 \pm 0.04	0.04	0.14 \pm 0.03	H I (1216)	2.1057	
20	3780.09 \pm 0.01	0.16	0.49 \pm 0.02	H I (1216)	2.1095	
21	3782.72 \pm 0.02	0.53	1.66 \pm 0.05	H I (1216)	2.1116	
22	3795.52 \pm 0.01	0.60	1.86 \pm 0.05	H I (1216)	2.1222	a
23	3821.93 \pm 0.01	0.19	0.57 \pm 0.03	Si II (1260)	2.0323	b
24	3847.53 \pm 0.22	-	0.25 \pm 0.04	not ident.		
25	3880.10 \pm 0.18	-	0.19 \pm 0.02	not ident.		
26	3885.27 \pm 0.06	0.08	0.22 \pm 0.05	Si IV (1393)	1.7876	c
27	3886.88 \pm 0.04	0.81	2.27 \pm 0.05	Si IV (1393)	1.7888	c
28	3904.40 \pm 0.15	-	0.22 \pm 0.04	not ident.		
29	3909.60 \pm 0.05	0.15	0.38 \pm 0.05	C IV (1548)	1.5253	d
30	3910.40 \pm 0.06	0.05	0.14 \pm 0.05	Si IV (1402)	1.7876	c
31	3912.02 \pm 0.04	0.57	1.60 \pm 0.08	Si IV (1402)	1.7888	c
32	3916.10 \pm 0.05	0.08	0.21 \pm 0.06	C IV (1550)	1.5253	d
33	3922.22 \pm 0.04	-	0.43 \pm 0.02	not ident.		
34	3925.67 \pm 0.04	-	0.40 \pm 0.07	not ident.		
35	4833.32 \pm 0.02	0.51	1.59 \pm 0.11	C IV (1548)	2.1219	a
36	4841.36 \pm 0.02	0.44	1.37 \pm 0.05	C IV (1550)	2.1219	a

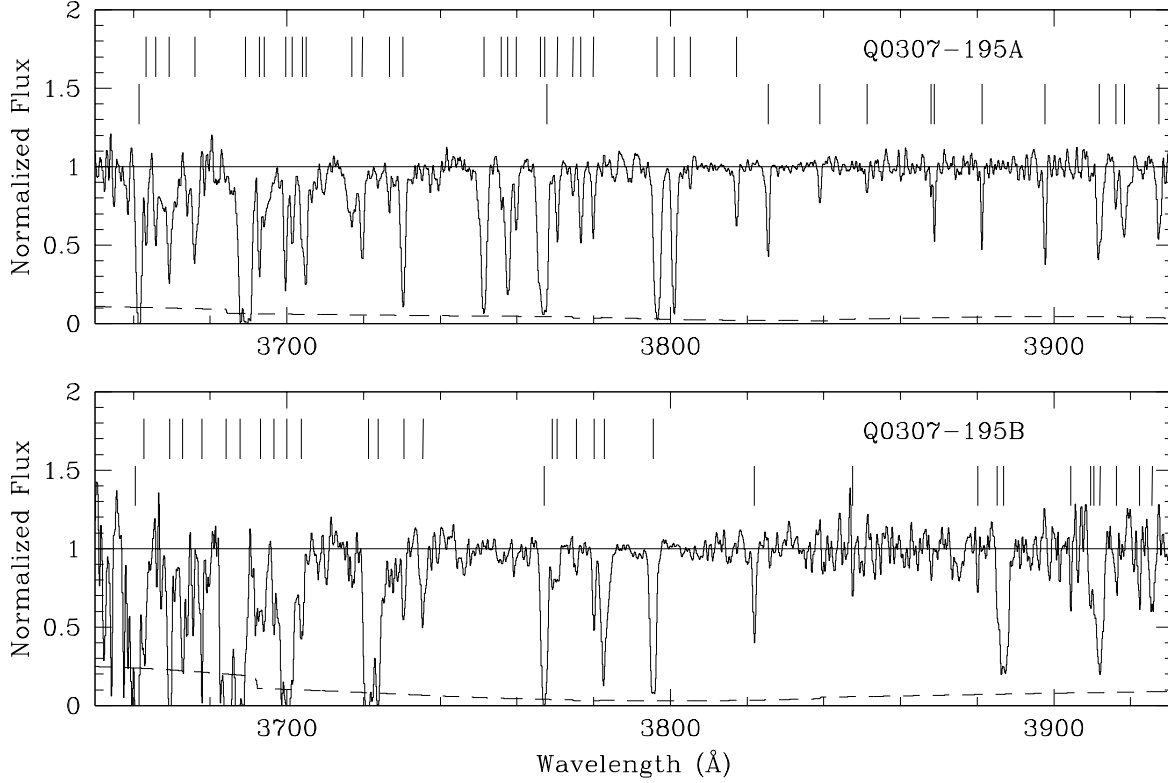


Fig. 1. Spectra of Q0307-195A,B obtained with the NTT EMMI instrument as a function of vacuum heliocentric wavelength. The dashed line shows the 1σ error in the flux. Tick marks indicate absorption lines detected at or above the 3.5σ confidence level, upper and lower tick marks are referred to Ly α and metal absorption lines respectively

The metal system at $z_{\text{abs}} = 2.0988 - b$

This is a new system. We identified the C IV and N V doublets in the red portion of the spectrum, and the Ly α line blended with the Si III 1207 of the previous system.

The metal systems at $z_{\text{abs}} = 2.03497 - c$ and $z_{\text{abs}} = 1.5267 - d$

Already observed by SR83. No new line has been added.

3.3. Object Q0307-195B

The metal systems at $z_{\text{abs}} = 2.1221 - a$ and $z_{\text{abs}} = 2.0333 - b$

Already observed by SR83. No new line has been added.

The metal system at $z_{\text{abs}} = 1.7882 - c$

Already observed by SR83. The identification is based only on the Si IV doublet, in the Ly α forest a possible C II can be identified but it is blended with a strong Ly α line. The Si IV doublet shows velocity structure and it was fitted with two components.

The metal system at $z_{\text{abs}} = 1.5253 - d$

The identification of this possible new system is based only on the C IV doublet found redward of the Ly α

emission line. This system differs in redshift by only 166 km s^{-1} from system *d* in object A.

All the lines in the Ly α forest not identified as metals are assumed to be Ly α .

4. The size of the Ly α absorbers

The main aim of this work is to determine the transverse size of the Ly α absorbers using the Ly α forests of the two adjacent LOSs of the pair. In order to avoid spurious effects due to the “proximity effect”, only the Ly α lines with velocity separation greater than 5000 km s^{-1} from the lower QSO redshift in the pair were considered in the sample.

The spectra of the observed pairs show a number of *hits*, \mathcal{N}_{h}^o , and of *misses*, \mathcal{N}_{m}^o . A *hit* occurs when an absorption line above a given threshold in rest equivalent width, W_o , appears in both QSO spectra, with a velocity difference less than a limit, Δv . A *miss* occurs when a line is seen in any of the QSO spectra, but no line above the W_o threshold is seen in the other.

A value $\Delta v = 200 \text{ km s}^{-1}$ has been adopted as the most suitable velocity window, being significantly larger than the resolution ($\sim 40 \text{ km s}^{-1}$) and close to the clus-

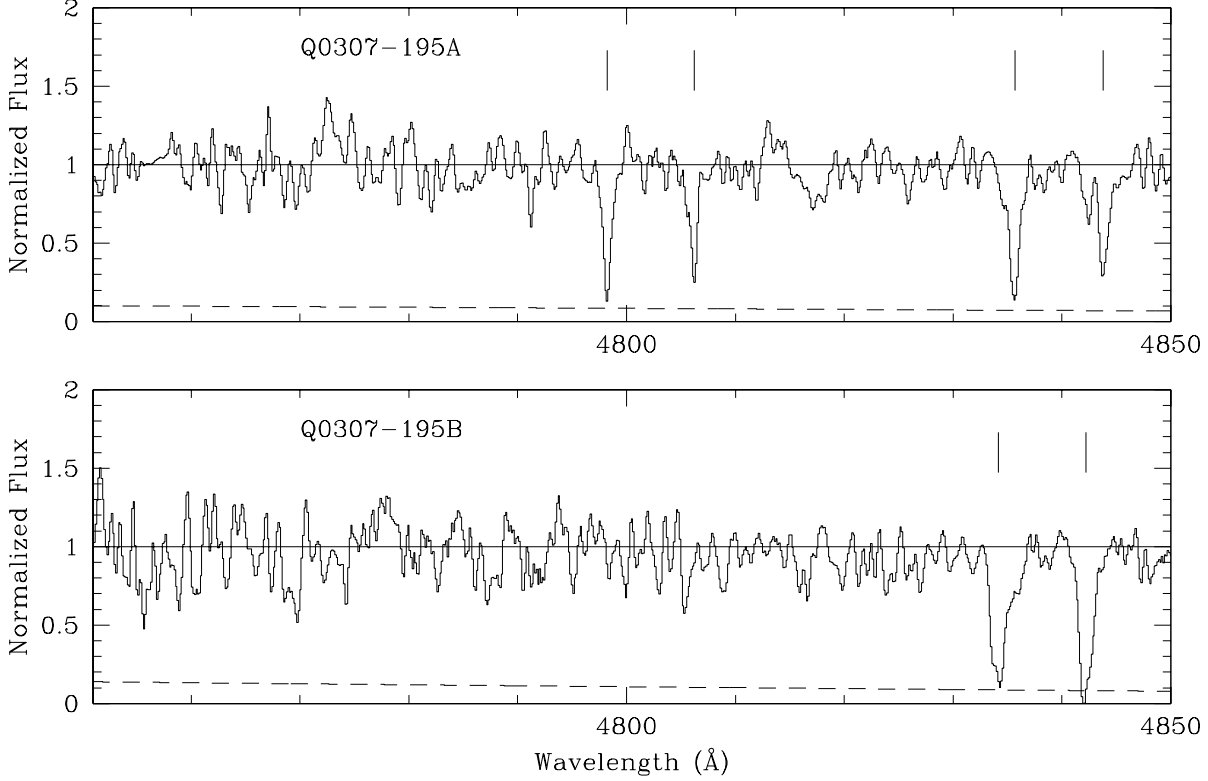


Fig. 2. Same as Fig. 1, for the CIV region

Table 3. Ly α lines that give rise to hits in the spectrum of Q0307-195A,B.

No.	λ_A (Obs.) (Å)	W_A (rest) (Å)	λ_B (Obs.) (Å)	W_B (rest) (Å)	$v_A - v_B$ (km s $^{-1}$)
1*	3669.36	0.33	3669.45	0.54	-7 ± 9
2	3676.08	0.32	3677.81	0.27	-141 ± 8
3*	3689.15	1.34	3687.80	1.19	110 ± 9
4	3694.16	0.23	3693.10	0.54	86 ± 16
5	3699.64	0.26	3700.04	1.25	-32 ± 4
6	3704.01	0.20	3703.81	0.28	16 ± 13
6	3704.98	0.22	3703.81	0.28	95 ± 8

* Hit in the case $w_o \geq 0.3$

tering scale observed for Ly α absorbers (Cristiani et al. 1997). As a consequence, all the Ly α lines in the sample whose separation was less than 200 km s $^{-1}$ have been merged into a single line with wavelength given by the average of the wavelengths and equivalent width equal to the sum of the equivalent widths of the “parent” lines.

In Table 3, the hits observed in the spectra of Q0307-195A,B are reported together with the velocity differences between the lines.

To constrain cloud sizes, it can be assumed that a binomial random process produces the observed number of hits and misses; if the probability for a hit is given by Ψ , the likelihood function of this binomial process is $\mathcal{L}(\mathcal{N}_h^o, \mathcal{N}_m^o | \Psi) = \Psi^{\mathcal{N}_h^o} (1 - \Psi)^{\mathcal{N}_m^o}$ (FDCB).

Ψ is the probability that both ray paths intersect the cloud, given that at least one ray path does. Ψ is related to the probability Φ , that one given LOS intersects the cloud given that the other adjacent ray path already does, by the formula:

$$\Psi = \Phi / (2 - \Phi). \quad (1)$$

The functional form of the probability Φ depends on the assumptions for the geometrical shape of the absorbers. In the hypothesis of single radius, spherical clouds, with the definition $X = S/2R$, where S is the proper separation of ray paths and R is the cloud radius, it is found (McGill 1990):

$$\Phi = (2/\pi) [\arccos X - X(1 - X^2)^{1/2}] \quad \text{for } X < 1, \quad (2)$$

Table 4. Parameters of the QSO pairs forming our enlarged sample and Ly α cloud radius estimates in the hypothesis of spherical and disc geometry

QSO Pair	Angular Separ. (arcsec)	Ly α z Range	S , Proper Separation (h^{-1} kpc)	W_0 cutoff (\AA)	\mathcal{N}_h^o	\mathcal{N}_m^o	<i>Spheres</i>		<i>Discs</i>	
							95% Confid. Interval in R (h^{-1} kpc)	Modal Radius (h^{-1} kpc)	95% Confid. Interval in R (h^{-1} kpc)	Modal Radius (h^{-1} kpc)
1343+2640A/B ¹	9.5	1.756-1.979	39-40	0.4	6	1	50-2705	80	70-3000	117
1026-0045A/B ²	36	0.833-1.398	149-155	0.2	5	15	98-268	137	117-385	179
				0.3	4	12	98-305	139	118-443	183
0307-195A/B ³	56	2.011-2.070	228-229	0.2	6	7	10-294	146	11-406	171
				0.3	2	9	< 269		< 365	
0107-025A/B ⁴	86	0.481-0.892	301-361	0.3	5	6	291-1776	475	379-2636	663
1517+2356/57 ⁵	102	1.390-1.787	427-438	0.4	3	21	34-460	277	39-618	330
1623+2651A/B ⁵	127	2.025-2.409	497-519	0.4	5	20	99-604	348	113-828	425
1623+2651A/53 ⁵	147	1.971-2.409	575-604	0.4	7	18	356-883	481	414-1247	619
1623+2653/51B ⁵	177	2.025-2.468	687-723	0.4	5	32	27-600	418	30-773	482

¹ Crofts et al. 1994² Petitjean et al. 1998³ This paper⁴ Dinshaw et al. 1997⁵ Crofts & Fang 1997

and $\Phi = 0$ otherwise.

As a second model, clouds can be idealized as circular discs, with a given radius R , much larger than their thickness, and an observed inclination angle θ . The probability that one ray path intersects the disc within the angle $\theta \rightarrow \theta + d\theta$, given that the other ray path already does, is (McGill 1990):

$$\Phi(\theta) = (\cos \theta / \pi) \left\{ \arccos \left(\frac{X}{\cos \theta} \right) - \left(\frac{X}{\cos \theta} \right) \times \left[1 - \left(\frac{X}{\cos \theta} \right)^2 \right]^{1/2} \right\} \quad \text{for } X < \cos \theta, \quad (3)$$

and $\Phi = 0$ otherwise. By integrating over θ for randomly oriented discs, the probability is then given by:

$$\Phi = \int_{-\pi/2}^{\pi/2} \Phi(\theta) d\theta. \quad (4)$$

In practice, from the observations we determine the numbers of hits and misses, \mathcal{N}_h^o and \mathcal{N}_m^o , and then we correct them for the accidental hits due to random velocity matches.

Two different procedures have been devised to compute the value of \mathcal{N}_h^o : in the first, the velocity separation between all the line pairs is computed and, when a given line combines to give more than one hit, only the one with the smallest velocity separation is taken into account, and the others are neglected. If, for example, lines 1 and 2 of spectrum A combine with lines 1 and 2 of spectrum B forming the couples 1-1, 1-2 and 2-2, and the couple 1-2

has the smallest velocity separation, we count just one hit. The second method takes the minimum value between the “A vs. B” hits and the “B vs. A” hits.

The two methods turned out to yield the same result in all the investigated cases.

The number of observed misses is given by the sum of the two \mathcal{N}_m^o ’s, “A vs. B” and “B vs. A”.

To take into account the possibility of *accidental hits* due to random velocity matches, we have used simulations of Poissonian distributions of absorption lines in the two QSO LOSs, with a number of lines in each spectrum equal to the observed one.

For each simulation we have computed:

- the number of accidental hits, \mathcal{N}_r , applying the same procedures used for the real spectra;
- the corrected number of hits, \mathcal{N}_h , (misses, \mathcal{N}_m) by subtracting \mathcal{N}_r from (adding $2\mathcal{N}_r$ to) the observed value.

Eventually, the probability distribution of the number of corrected hits $\mathcal{C}(\mathcal{N}_h)$ was evaluated. The probability $\mathcal{C}(0)$ takes into account all the occurrences with $\mathcal{N}_r \geq \mathcal{N}_h^o$.

For each pair of values of corrected hits and misses, given the expressions for the probability distributions Φ and Ψ , it is possible to apply Bayes’s Theorem (Press 1989, FDCB) to yield the a posteriori probability density for the radius R ,

$$\mathcal{P}(R, \mathcal{N}_h, \mathcal{N}_m) = \frac{\mathcal{L}(\mathcal{N}_h, \mathcal{N}_m | \Psi) f(R)}{\int_0^\infty \mathcal{L}(\mathcal{N}_h, \mathcal{N}_m | \Psi) f(R) dR}. \quad (5)$$

At variance with FDCB, we have chosen as a prior distribution, $f(R)$, a uniform distribution for R between 0 and R_{\max} , and not a uniform distribution of $\Psi(R)$.

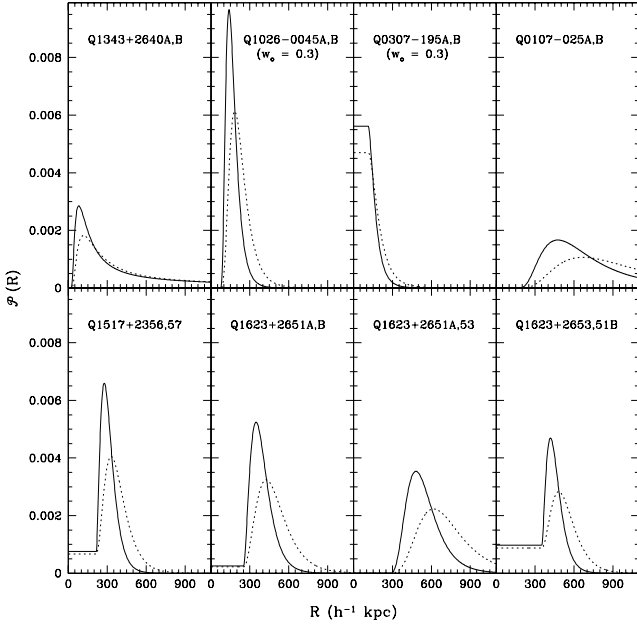


Fig. 3. Probability distribution $\mathcal{P}(R)$ as given by eq. (8) for spherical absorbers (*solid curve*) and randomly inclined discs (*dotted curve*) as functions of cloud radius for all the QSO pairs considered in the paper. The plateau at separation below $S/2$ arises because there is a non-vanishing probability that the number of corrected hits be 0 ($\mathcal{C}(0) \neq 0$)

It is worth stressing that a uniform prior distribution for the probability Ψ introduces a cutoff at high and low R that forces the 95 % confidence intervals to be narrow also in situations with a very low number of hits or misses. In particular, a spurious dependence of R on the proper separation S is induced in the case of very few hits, which is the common situation at large separations, because the probability $\Psi(R)$ actually depends on S . Since there is no particular justification to assume a uniform $\Psi(R)$, we have chosen a uniform distribution for R which does not introduce biases in the results.

Equation (5) then becomes

$$\mathcal{P}(R, \mathcal{N}_h, \mathcal{N}_m) = \frac{\mathcal{L}(\mathcal{N}_h, \mathcal{N}_m | \Psi)}{\int_0^{R_{\max}} \mathcal{L}(\mathcal{N}_h, \mathcal{N}_m | \Psi) dR}. \quad (6)$$

We have adopted as R_{\max} a value of $3 h^{-1}$ Mpc which represent the *mean free path* between two absorbers along the line of sight, as obtained from the line distribution $\partial^2 n / \partial z \partial N_{\text{HI}}$ (Giallongo et al. 1996) at a redshift $z \sim 2$, in the column density range $14 \leq \log N_{\text{HI}} \leq 17$.

In the case of discs, the maximum value is increased by a factor $\sqrt{2}$, yielding a value $R_{\max} \simeq 4 h^{-1}$ Mpc.

It has to be noted that the value of this maximum radius does not influence in practice the resulting modal

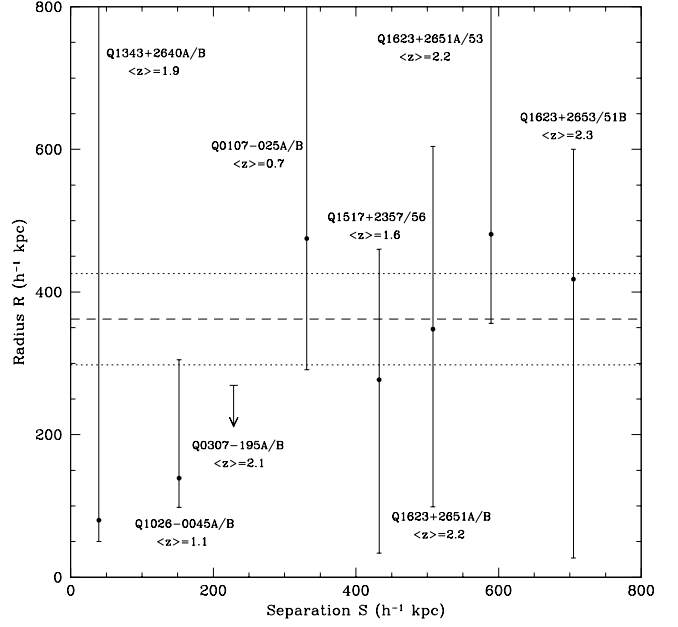


Fig. 4. Inferred cloud radius R (and 95 % confidence interval) from a model assuming single-radius, unclustered spherical clouds, as a function of QSO pair sightline separation S . The dashed line shows the most probable value for R and the dotted lines the 95 % confidence interval (see text)

radii and confidence intervals, because the probability distributions for R usually go to zero well before this upper limit. R_{\max} plays a significant role only if the number of misses is extremely low (1 or 0).

In the case of no hits, recipe (6) gives an incorrect result, in fact, the probability Φ becomes zero for $R < S/2$ by definition. In this extreme occurrence we have then to write:

$$\mathcal{P}(R, \mathcal{N}_h, \mathcal{N}_m) = A \times \begin{cases} 1 & \text{if } R < S/2 \\ \mathcal{L}(\mathcal{N}_h, \mathcal{N}_m | \Psi) & \text{if } R \geq S/2 \end{cases} \quad (7)$$

where, A is the proper normalization factor which makes $\int_0^{R_{\max}} \mathcal{P}(R, \mathcal{N}_h, \mathcal{N}_m) = 1$.

The global $\mathcal{P}(R)$ for a given QSO pair is finally obtained by the sum:

$$\mathcal{P}(R) = \sum \mathcal{P}(R, \mathcal{N}_h, \mathcal{N}_m) \times \mathcal{C}(\mathcal{N}_h). \quad (8)$$

In order to investigate the possible correlations of the radius R with the LOS separation and with the redshift, we have applied our analysis to 7 other data samples of comparable quality, published in the literature: Q1343+2640A,B (Crofts et al. 1994), Q1026-0045A,B (Petitjean et al. 1998), Q0107-025A,B (D97), Q1517+2356,1517+2357 (CF97),

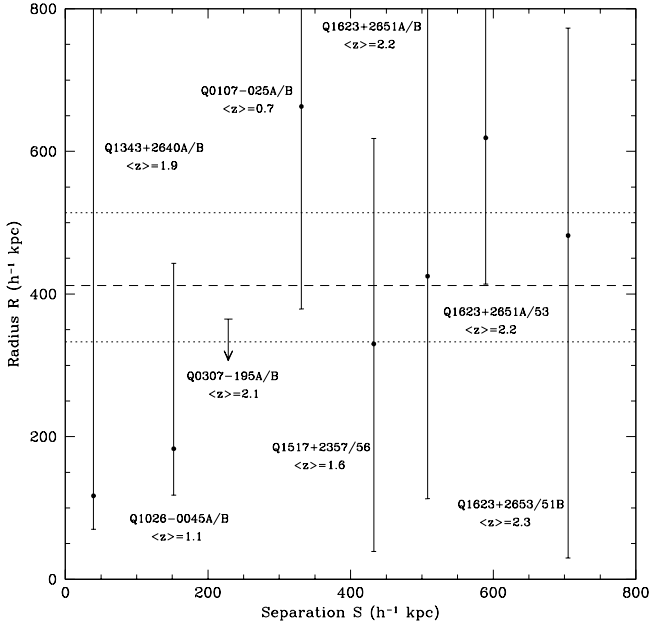


Fig. 5. Same as Fig. 4 but for single-radius, unclustered thin discs

Q1623+2651A,1623+2653,1623+2651B (CF97). The QSO pair Q1343+2640A,B has been observed also by Dinshaw et al. (1994), we have chosen to use Crotts et al. (1994) line list because of the larger wavelength coverage and larger number of identified lines.

The relevant information are displayed in Table 4. Columns 6 and 7 report the observed number of hits and misses, respectively.

The most probable number of accidental hits for each QSO pair is: 0 for 1343+2640A,B; 0 for 1026-0045A,B (for both $W_o = 0.2$ and $W_o = 0.3$); 2 for 0307-195A,B ($W_o = 0.3$); 6 for 0307-195A,B ($W_o = 0.2$); 0 for 0107-025A,B; 1 for 1517+2356/57; 2 for 1623+2651A,B; 2 for 1623+2651A/53 and 5 for 1623+2653,51B.

In the actual computation of the cloud sizes the average value of the proper separation has been adopted.

In Fig. 3 the probability distributions given by equation (8) for all the QSO pairs presented in the paper are plotted for the two cases of spherical and disc geometry.

In Fig. 4 and Fig 5 the values estimated for the modal radii are plotted as a function of S . We consider that if the typical radius $R_{50} \leq S/2$, where R_{50} is defined as

$$\int_0^{R_{50}} \mathcal{P}(R) = 0.5, \quad (9)$$

only an upper limit can be set to the dimension of the absorber. This is the case for Q0307-195A,B (with $W_o \geq 0.3$ Å) for which $R_{50} \simeq 90 h^{-1} \text{ kpc} < 114 h^{-1} \text{ kpc}$ for the spherical model and $R_{50} \simeq 107 h^{-1} \text{ kpc} < 114 h^{-1} \text{ kpc}$ for the disc model. The dashed line represents the most

probable modal radius, $R = 362 h^{-1} \text{ kpc}$, with 95% confidence limits $298 < R < 426 h^{-1} \text{ kpc}$ (spherical absorbers) and $R = 412 h^{-1} \text{ kpc}$, with 95% confidence limits $333 < R < 514 h^{-1} \text{ kpc}$ (disc). These values correspond to the peak of the total probability density obtained as the product of the probability densities of the considered QSO pairs.

A plot of the modal radius as a function of the average redshift of the Ly α forest of the corresponding QSO pair does not show any correlation between the two, at variance with the result obtained by Dinshaw et al. (1998).

The quality of the present data on the pair Q0307-195A,B and of the data by Petitjean et al. (1998) for the pair Q1026-0045A,B allows defining a complete sample of lines down to an equivalent width $W_o = 0.2$ Å. The resulting number of hits and misses, the radius and confidence interval are reported in Table 4. The corresponding values of the global modal radius and 95 % confidence interval are $R = 350 h^{-1} \text{ kpc}$ and $276 < R < 417 h^{-1} \text{ kpc}$ (sphere), $R = 408 h^{-1} \text{ kpc}$ and $325 < R < 501 h^{-1} \text{ kpc}$ (disc).

Until fairly recently it has been conjectured that the typical transverse sizes of the Ly α were of the order of a few tens of kpc. The present analysis indicates about one order of magnitude larger dimensions at $z \sim 2$, implying correspondingly larger ionizations and masses. With the presently inferred sizes and the typical UV background conditions at $z \sim 2$ (Giallongo et al. 1996), optically thin absorbers of $\log(N_{\text{HI}}) \sim 14 - 15$ are expected to show a remarkably small fraction of neutral Hydrogen, roughly $10^{-5.5} - 10^{-5}$. In this way the mean intergalactic density contributed by these clouds (Hu et al. 1995), especially in the spherical case, is close to conflict with the baryon limit from nucleosynthesis $\Omega_b \leq 0.015 h^{-2}$ (Walker et al. 1991). This potential incongruity can however be alleviated by assuming a disc or other geometries.

4.1. Towards more realistic models

The approach described in the previous section, although customarily used to determine the size of the Ly α absorbers, is expected to give just a rough idea of the dimension of these structures, due to the simplistic hypotheses made on their geometry.

In particular, the information on the equivalent width of the lines are not taken into account, since no density distribution is assumed inside the absorbers. Besides, all the clouds are assumed to have the same radius.

In the literature (Smette et al. 1992; Smette et al. 1995; Charlton et al. 1997; Dinshaw et al. 1997) this problem has been tackled adopting a statistical technique that utilizes the information about the equivalent width of the lines.

Dinshaw et al. (1997) adopted a power-law column density profile for the absorbers, $N(r) = N_{\text{lim}}(r/R_0)^{-\gamma}$, where $N_{\text{lim}} = 1.26 \times 10^{14} \text{ cm}^{-2}$ for $b = 35 \text{ km s}^{-1}$ is the limiting column density of the sample, R_0 is the radius of the absorber at $N = N_{\text{lim}}$ and $\gamma = 4$, and three simple

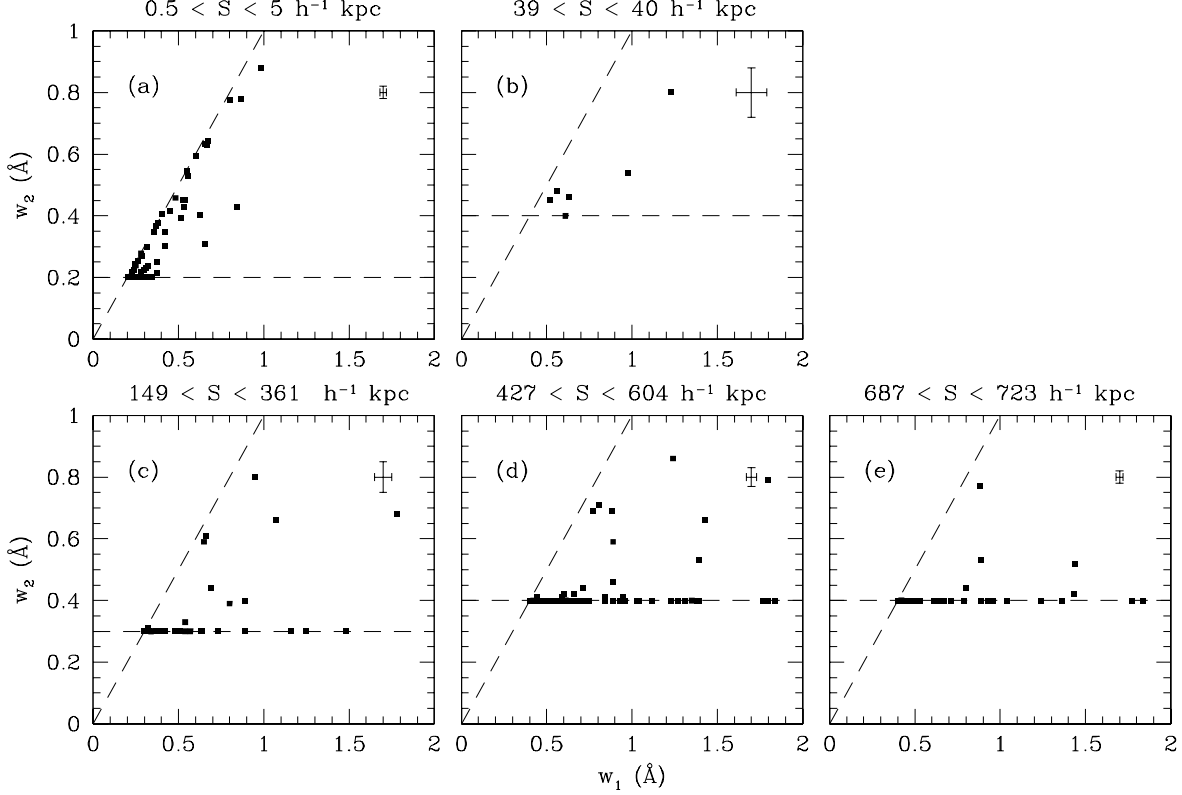


Fig. 6. Equivalent widths of the hits and misses for the 8 QSO pairs in our sample plus the data by Smette et al. (1995), they are grouped as follows: (a) HE1104-1805; (b) Q1343+2640A,B; (c) Q1026-0045A,B Q0307-195A,B and Q0107-025A,B; (d) Q1517+2356,1517+2357 Q1623+2651A,B and Q1623+2651A,1623+2653; (e) Q1623+2653,1623+2651B. The equivalent widths are arranged such that $W_1 \equiv \max(W_A, W_B)$ and $W_2 \equiv \min(W_A, W_B)$. The horizontal dashed lines represent the rest equivalent width threshold: $W_o > 0.2$ for (a), $W_o > 0.3$ for (b), (c) and $W_o > 0.4$ for (d), (e). The error bars in the upper right corners of the plots represents the average 1σ errors for the equivalent width

geometries with fixed radius: spheres, randomly inclined discs, and pseudo-filamentary structures (approximated as discs with fixed inclination $\cos i = 0.2$).

The column density distribution along paired lines of sight for each of the geometric models considered is simulated by means of the Monte Carlo techniques outlined by Smette et al. (1992). This distribution can be converted into the corresponding equivalent width distribution adopting an approximation to the curve of growth (Chernomordik & Ozernoy 1993).

In Fig. 6 the equivalent widths of the hits and misses are plotted for an enlarged sample of QSO pairs formed by our previously described 8 cases plus the lensed QSO HE 1104-1805A,B observed by Smette et al. (1995). The pairs are grouped according to their typical proper separation. It should be noted that it is now certain that the double QSO HE 1104-1805A,B is actually a gravitational lens system, as the lensing galaxy has been detected (Courbin et al. 1998; Remy et al. 1998). The exact values of the separation between the two light beams depend on the still badly determined lens redshift. The values we reported in Fig. 6 have been estimated using Fig. 6 of the paper by

Smette et al. (1995), for the redshift $z_{\text{lens}} = 1.32$, favoured by Remy et al. (1998).

It is clear from the figure that the fraction of hits decreases as the proper separation increases, while, at the same time, the correlation between the equivalent widths of the absorbers in the two LOS becomes poorer and poorer.

The present observations can be compared with the simple model predictions of D97 (their Fig. 12). In particular, our Fig. 6(a) shows reasonable agreement with the prediction of a disc model with $R_0 \sim 7 S$ that is $R_0 \sim 90 h^{-1}$ kpc; panel (b) agrees with the case $R_0 = 2 - 3 S$ for both filament and disc model, that is $R_0 \simeq 80 - 120 h^{-1}$ kpc; panel (c) can be explained by filaments and disc with $R_0 = S$ which implies $R_0 \sim 220 h^{-1}$ kpc and, finally, panels (d) and (e) agrees with filament and disc models with $R_0 \leq S$ or $R_0 \lesssim 500 - 700 h^{-1}$ kpc. Altogether a disc geometry with $R_0 \sim 100 - 200 h^{-1}$ kpc seems to be favored.

It should be noted, however, that the number of degrees of freedom is not the same in the three models: once

a given radius is chosen in the disc idealization the two orientation angles can vary at random, for the filament geometry one angle is fixed, and for the sphere no angular variable exists to define an orientation. In this way, it is obviously easier for the disc model to reproduce the real data that show a substantial amount of scatter due to measurement errors and possibly to a non-unique value of the cloud size.

In fact, by introducing one more degree of freedom in the spherical cloud model: i.e. allowing the radius R to vary according to one of the two distribution: (1) exponential, and (2) power law with indices $\alpha = -4, -3, \dots, 5, 6$, it is found that a power law distribution with $\alpha = 3$ provides an equally reasonable representation of the observed equivalent width distribution (D97).

5. Conclusions

We have presented new spectra of the quasar pair Q0307-195A,B.

The number of detected lines is almost doubled with respect to the previous study of this pair (Shaver & Robertson 1983). One new metal system has been identified in object A on the basis of the C IV doublet and one possible system is found also in object B.

In order to study the shape and dimension of the Ly α absorbers, we have added to the observations of the present QSO pair, data of comparable resolution taken from the literature to create a sample of 8 QSO pairs. We looked for hits and misses in the pair spectra and computed the probability distribution for a given radius R in the case of spherical and disc geometry basing our statistical analysis on the approach outlined by Fang et al. (1996). We modified some of their assumptions in order to deal correctly with the extreme cases of very low numbers (1 or 0) of hits or misses and avoid any spurious dependence on the separation between lines of sight.

Our results can be summarized as follows:

- the total probability density obtained as the product of the probability densities of the considered QSO pairs, gives a modal radius $R = 362 h^{-1}$ kpc, with 95% confidence limits $298 < R < 426 h^{-1}$ kpc (spherical absorbers) and $R = 412 h^{-1}$ kpc, with 95% confidence limits $333 < R < 514 h^{-1}$ kpc (disc).
- No significant correlation is detected between the modal radius and the mean proper separation of the pair, nor between the modal radius and the mean redshift of the Ly α forest region.
- The comparison of the distribution of the equivalent widths of the observed coincident lines with the predictions of Monte Carlo simulations for three simple geometrical models, spheres, discs and filaments with a power-law column density profile $N(r) \propto (r/R_0)^{-\gamma}$ (Dinshaw et al. 1997), seems to indicate a disc shape with $R_0 \sim 100 - 200 h^{-1}$ kpc and $\gamma \sim 4$ as the most

suitable. This could however be simply the result of the different number of parameters in the three models. If, for example, a further degree of freedom is allowed to the model based on spheres in the form of a power-law distribution of radii, a satisfactory consistency with the data is obtained.

Acknowledgements. We are grateful to J. Bergeron for enlightening suggestions. We thank the referee, Dr. A. Smette, for the stimulating comments. SC acknowledges the support of the ASI contract ARS-96-176 and of the Formation and Evolution of Galaxies network set up by the European Commission under contract ERB FMRX-CT96-086 of its TMR programme.

References

- Bajtlik, S., Duncan, R.C., Ostriker, J.P., 1988, ApJ 327, 570
 Bechtold, J., Crofts, A.P.S., Duncan, R.C., et al., 1994, ApJ 437, L83
 Charlton, J.C., Anninos, P., Zhang, Y., et al., 1997, ApJ 485, 26
 Chernomordik, V.V., Ozernoy, L.M., 1993, ApJ 404, L5
 Courbin, F., Lidman, C., Magain, P., 1998, A&A 330, 57
 Cristiani, S., D’Odorico, S., D’Odorico, V., et al., 1997, MNRAS 285, 209
 Crofts, A.P.S., 1985, ApJ 298, 732
 Crofts, A.P.S., 1989, ApJ 336, 550
 Crofts, A.P.S., Bechtold, J., Fang, Y., et al., 1994, ApJ 437, L79
 Crofts, A.P.S., Fang, Y., 1997, preprint astro-ph/9702185
 Dinshaw, N., Foltz, C.B., Impey, C.D., et al., 1998, ApJ 494, 567
 Dinshaw, N., Foltz, C.B., Impey, C.D., et al., 1995, Nature 373, 223
 Dinshaw, N., Impey, C.D., 1996, ApJ 458, 73
 Dinshaw, N., Impey, C.D., Foltz, C.B., et al., 1994, ApJ 437, L87
 Dinshaw, N., Weymann, R.J., Impey, C.D., et al., 1997, ApJ 491, 45
 Elowitz, R.M., Green, R.F., Impey, C.D., 1995, ApJ 440, 458
 Fang, Y., Duncan, R.C., Crofts, A.P.S., et al., 1996, ApJ 462, 77
 Foltz, C.B., Weymann, R.J., Roser, H.J., et al., 1984, ApJ 281, L1
 Giallongo, E., Cristiani, S., D’Odorico, S., et al., 1996, ApJ 466, 46.
 Hu, E. M., Kim, T., Cowie, L. L., et al., 1995, AJ 110, 1526
 Jakobsen, P., Perryman, M.A.C., Di Serego Alighieri, S., et al., 1986, ApJ 303, L27
 MacAlpine, G.M., Feldman, F.R., 1982, ApJ 261, 412
 McGill, C., 1990, MNRAS 242, 544
 Petitjean P., Surdej, S., Smette, A., et al., 1998, A&A 334, L45
 Press, S.J., 1989, Bayesian Statistics: Principles, Models & Applications, Wiley, New York
 Remy, M., et al. 1998, New Astronomy, in press
 Shaver, P.A., Robertson, J.G. 1983, ApJ 268, L57
 Smette, A., Surdej, J., Shaver, P.A., et al., 1992, ApJ 389, 39
 Smette, A., Robertson, J.G., Shaver, P.A., et al., 1995, A&AS 113, 199
 Tytler, D., Sandoval, J., Fan, X.-M., 1993, ApJ 405, 57

- Walker, T. P., Steigman, G., Schramm, D. N., et al., 1991, ApJ 376, 51
- Weymann, R.J., Foltz, C.B., 1983, ApJ 272, L1
- Williger, G.M., Hazard, C., Baldwin, J.A., et al., 1996, ApJS 104, 145
- Young, P.J., Sargent, W.L.W., Boksenberg, A., et al., 1979, ApJ 229, 891